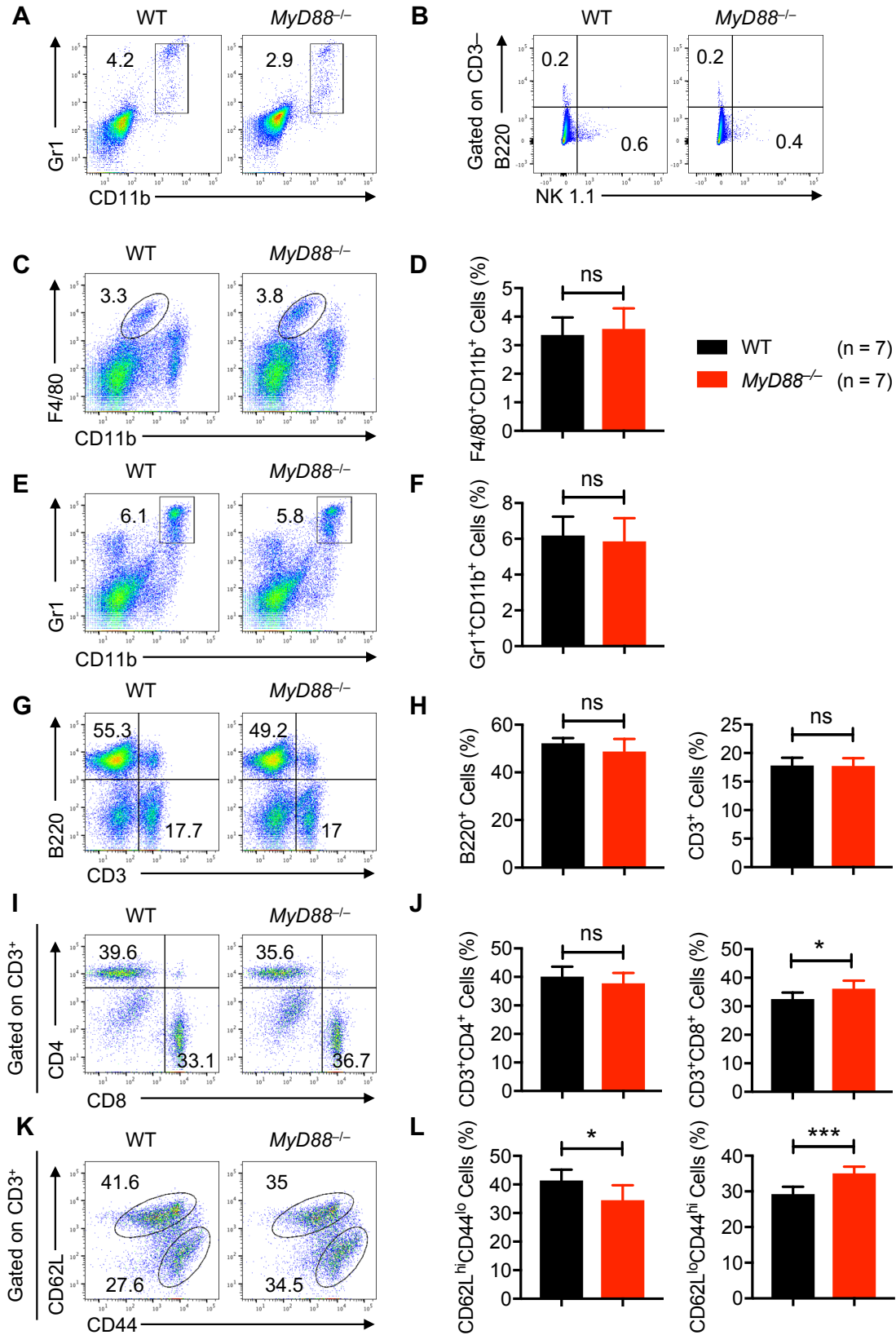


**Supplementary Figure S1: *Trif* is dispensable for melanoma tumor progression.**

**A–D**, B16-F10 melanoma cells were injected into WT and *Trif*<sup>-/-</sup> mice. **(A)** Mean tumor volume in WT (n = 15) and *Trif*<sup>-/-</sup> (n = 10) mice. **(B)** Tumor weights of WT (n = 15) and *Trif*<sup>-/-</sup> (n = 10) mice, 2 weeks after tumor cell injection. **(C)** Representative pictures of tumors from WT and *Trif*<sup>-/-</sup> mice. **(D)** Immunohistochemistry staining of tumors with F4/80 harvested from WT (n = 5) and *Trif*<sup>-/-</sup> (n = 5) mice. (Scale bar, 100 μm).

Data are presented as mean ± SD. **(A)** Two-way ANOVA with Sidak's multiple comparison test and **(B)** unpaired *t*-test with Welch's correction were used to determine the significance between the two groups analyzed. ns, not significant \*\**P* < 0.01.



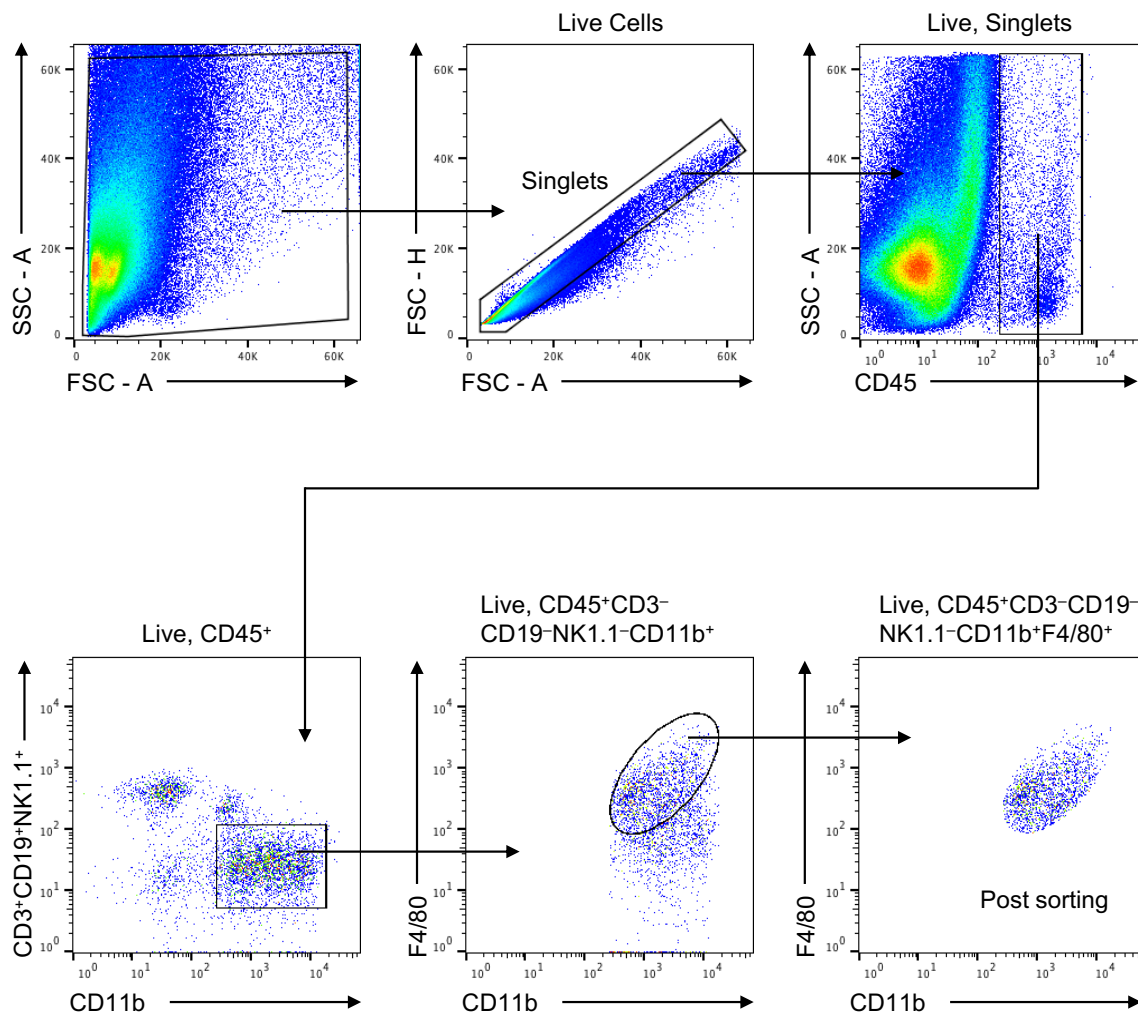
Supplementary Figure S2: Tumor and splenic immune cell populations in *MyD88*<sup>-/-</sup> mice

**bearing melanoma.**

**A–B**, Flow cytometry analysis of immune cell populations in tumors harvested from WT (n = 7) and *MyD88*<sup>-/-</sup> (n = 7) mice. **(A)** Pseudocolor plots of the Gr1<sup>+</sup>CD11b<sup>+</sup> granulocyte population. **(B)** Pseudocolor plots of B220<sup>+</sup> B-cell and NK1.1<sup>+</sup> NK-cell populations.

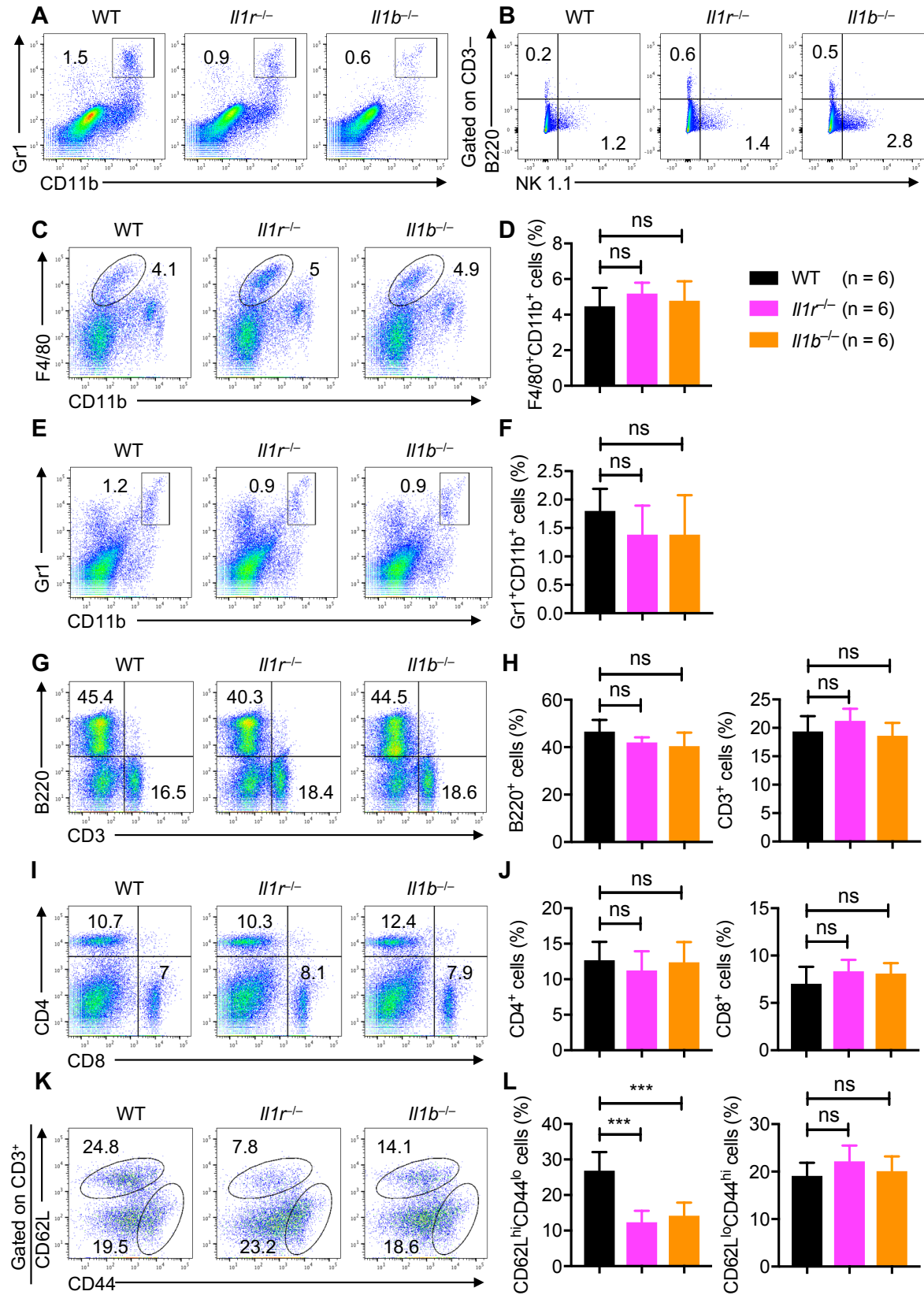
**C–L**, Flow cytometry analysis of immune cell populations in spleens harvested from WT (n = 7) and *MyD88*<sup>-/-</sup> (n = 7) mice. **(C)** Pseudocolor plots of F4/80<sup>+</sup>CD11b<sup>+</sup> macrophage population. **(D)** Quantification of the F4/80<sup>+</sup>CD11b<sup>+</sup> macrophage population. **(E)** Pseudocolor plots of the Gr1<sup>+</sup>CD11b<sup>+</sup> granulocyte population. **(F)** Quantification of the Gr1<sup>+</sup>CD11b<sup>+</sup> granulocyte population. **(G)** Pseudocolor plots of the B220<sup>+</sup> B-cell and CD3<sup>+</sup> T-cell populations. **(H)** Quantification of the B220<sup>+</sup> B-cell and CD3<sup>+</sup> T-cell populations. **(I)** Pseudocolor plots of the CD3<sup>+</sup>CD4<sup>+</sup> and CD3<sup>+</sup>CD8<sup>+</sup> T-cell populations. **(J)** Quantification of the CD3<sup>+</sup>CD4<sup>+</sup> and CD3<sup>+</sup>CD8<sup>+</sup> T-cell populations. **(K)** Pseudocolor plots of the CD62L<sup>hi</sup>CD44<sup>lo</sup> naïve and CD62L<sup>lo</sup>CD44<sup>hi</sup> effector T-cell populations. **(L)** Quantification of the CD62L<sup>hi</sup>CD44<sup>lo</sup> naïve and CD62L<sup>lo</sup>CD44<sup>hi</sup> effector T-cell populations.

Data are presented as mean ± SD. Unpaired *t*-test, with Welch's correction, was used to determine the statistical significance between the two groups analyzed. ns, not significant, \**P* < 0.05, \*\*\**P* < 0.001.



**Supplementary Figure S3: FACS gating strategy for sorting the TAM population in tumors.**

Debris and doublets were removed, then TAMs were sorted as the CD45<sup>+</sup>CD3<sup>-</sup>CD19<sup>-</sup>NK1.1<sup>-</sup>CD11b<sup>+</sup>F4/80<sup>+</sup> population.



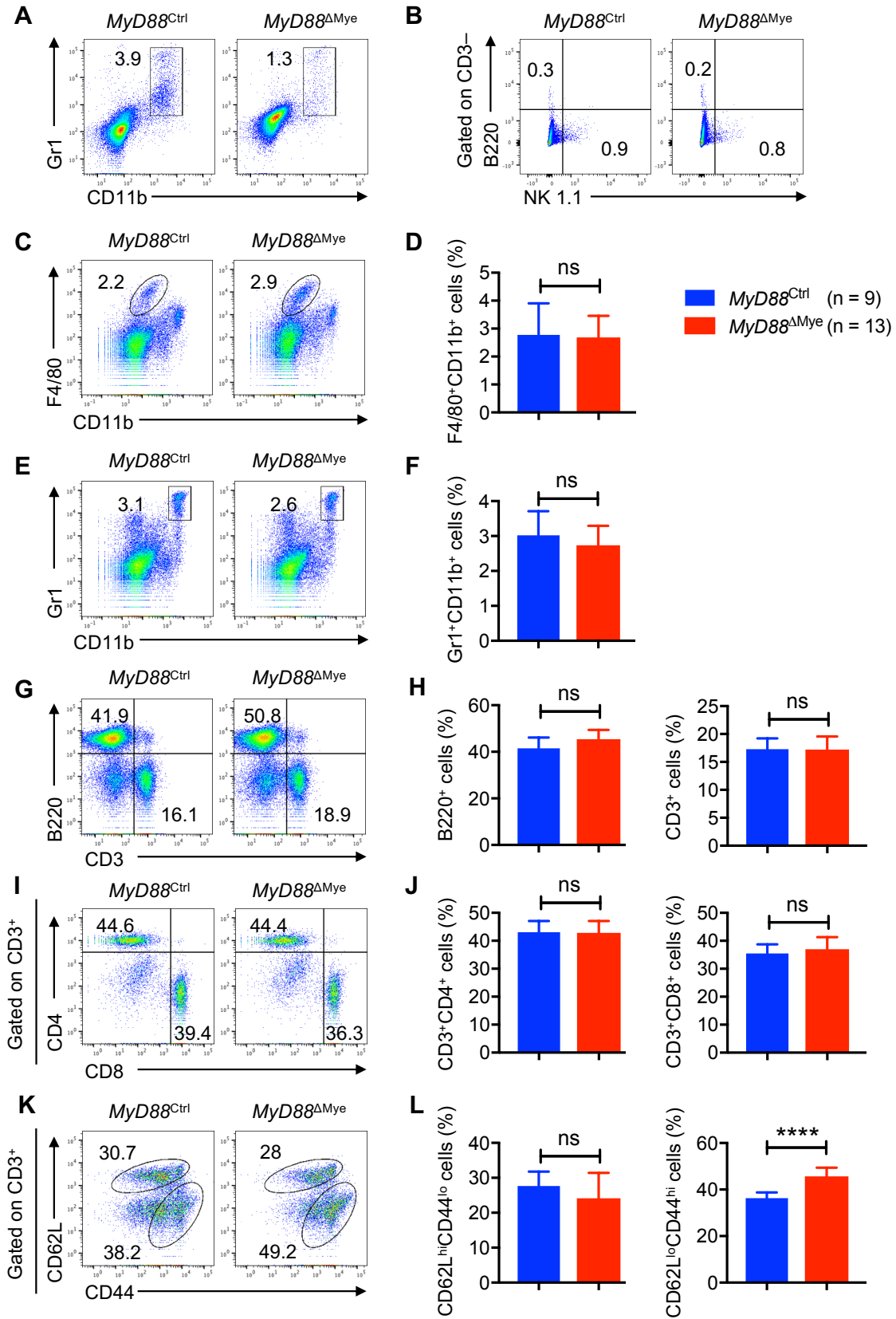
Supplementary Figure S4: Tumor and splenic immune cell populations in IL-1R<sup>-</sup> or IL-1 $\beta$ <sup>-</sup>

**deficient mice bearing melanoma.**

**A–B**, Flow cytometry analysis of immune cell populations in tumors harvested from WT (n = 6), *Il1r<sup>-/-</sup>* (n = 6) and *Il1b<sup>-/-</sup>* (n = 6) mice. **(A)** Pseudocolor plots of the Gr1<sup>+</sup>CD11b<sup>+</sup> granulocyte population. **(B)** Pseudocolor plots of B220<sup>+</sup> B-cell and NK1.1<sup>+</sup> NK-cell populations.

**C–L**, Flow cytometry analysis of immune cell populations in spleens harvested from WT (n = 6), *Il1r<sup>-/-</sup>* (n = 6) and *Il1b<sup>-/-</sup>* (n = 6) mice. **(C)** Pseudocolor plots of the F4/80<sup>+</sup>CD11b<sup>+</sup> macrophage population. **(D)** Quantification of the F4/80<sup>+</sup>CD11b<sup>+</sup> macrophage population. **(E)** Pseudocolor plots of the Gr1<sup>+</sup>CD11b<sup>+</sup> granulocyte population. **(F)** Quantification of the Gr1<sup>+</sup>CD11b<sup>+</sup> granulocyte population. **(G)** Pseudocolor plots of the B220<sup>+</sup> B-cell and CD3<sup>+</sup> T-cell populations. **(H)** Quantification of the B220<sup>+</sup> B-cell and CD3<sup>+</sup> T-cell populations. **(I)** Pseudocolor plots of the CD4<sup>+</sup> and CD8<sup>+</sup> T-cell populations. **(J)** Quantification of the CD4<sup>+</sup> and CD8<sup>+</sup> T-cell populations. **(K)** Pseudocolor plots of the CD62L<sup>hi</sup>CD44<sup>lo</sup> naïve and CD62L<sup>lo</sup>CD44<sup>hi</sup> effector T-cell populations. **(L)** Quantification of the CD62L<sup>hi</sup>CD44<sup>lo</sup> naïve and CD62L<sup>lo</sup>CD44<sup>hi</sup> effector T-cell populations.

Data are presented as mean ± SD. Unpaired *t*-test, with Welch's correction, was used to determine the statistical significance between the two groups analyzed. ns, not significant, \*\*\**P* < 0.001.



Supplementary Figure S5: Tumor and splenic immune cell populations in *MyD88*<sup>ΔMyc</sup> mice



**bearing melanoma.**

**A–B**, Flow cytometry analysis of immune cell populations in tumors harvested from *MyD88<sup>Ctrl</sup>* (n = 9) and *MyD88<sup>ΔMye</sup>* (n = 13) mice. **(A)** Pseudocolor plots of the Gr1<sup>+</sup>CD11b<sup>+</sup> granulocyte population. **(B)** Pseudocolor plots of B220<sup>+</sup> B-cell and NK1.1<sup>+</sup> NK-cell populations.

**C–L**, Flow cytometry analysis of immune cell populations in spleens harvested from *MyD88<sup>Ctrl</sup>* (n = 9) and *MyD88<sup>ΔMye</sup>* (n = 13) mice. **(C)** Pseudocolor plots of the F4/80<sup>+</sup>CD11b<sup>+</sup> macrophage population. **(D)** Quantification of the F4/80<sup>+</sup>CD11b<sup>+</sup> macrophage population. **(E)** Pseudocolor plots of the Gr1<sup>+</sup>CD11b<sup>+</sup> granulocyte population. **(F)** Quantification of the Gr1<sup>+</sup>CD11b<sup>+</sup> granulocyte population. **(G)** Pseudocolor plots of the B220<sup>+</sup> B-cell and CD3<sup>+</sup> T-cell populations. **(H)** Quantification of the B220<sup>+</sup> B-cell and CD3<sup>+</sup> T-cell populations. **(I)** Pseudocolor plots of the CD3<sup>+</sup>CD4<sup>+</sup> and CD3<sup>+</sup>CD8<sup>+</sup> T-cell populations. **(J)** Quantification of the CD3<sup>+</sup>CD4<sup>+</sup> and CD3<sup>+</sup>CD8<sup>+</sup> T-cell populations. **(K)** Pseudocolor plots of the CD62L<sup>hi</sup>CD44<sup>lo</sup> naïve and CD62L<sup>lo</sup>CD44<sup>hi</sup> effector T-cell populations. **(L)** Quantification of the CD62L<sup>hi</sup>CD44<sup>lo</sup> naïve and CD62L<sup>lo</sup>CD44<sup>hi</sup> effector T-cell populations.

Data are presented as mean ± SD. Unpaired *t*-test, with Welch's correction, was used to determine the statistical significance between the two groups analyzed. ns, not significant, \*\*\*\**P* < 0.0001.

**Supplementary Table S1: Average FPKM values of genes in the study analyzed in various cancers.**

	<b>Melanoma</b> n = 102	<b>Breast Cancer</b> n = 1075	<b>Colorectal Cancer</b> n = 597	<b>Ovarian Cancer</b> n = 373	<b>Lung Cancer</b> n = 994	<b>Stomach Cancer</b> n = 354
<b><i>MYD88</i></b>	16.2	18.3	22.5	18.6	17.5	26
<b><i>TIRAP</i></b>	2.3	2.6	2.3	1.3	2.1	3.6
<b><i>TICAM1</i></b>	10.5	10.6	14.9	10.4	11.4	18.3
<b><i>TICAM2</i></b>	0	0	0	0	0	0